

## Structures and Energetics of $\text{SrFeO}_{2.875}$ Calculated within the GGA + $U$ Framework

Wen Lai Huang\* and Qingshan Zhu

State Key Laboratory of Multi-Phase Complex Systems, Institute of Process Engineering,  
 Chinese Academy of Sciences, Beijing 100190, People's Republic of China

Received August 4, 2009

**Abstract:** The energetics and electronic properties of  $\text{SrFeO}_{2.875}$  have been systematically calculated with the fully relaxed atomic positions at both GGA and GGA +  $U$  levels, and different spin-polarized configurations have been considered. Many atoms besides the nearest neighbors of the oxygen vacancy have been found to be influenced by the vacancy in terms of positions and electronic structures. The obtained magnetic moments suggest the high-spin character of the Fe 3d electrons, in combination with the larger exchange splitting compared with the crystal field splitting. The local states at the Fermi level are found to be situated within the  $\pi^*$  band in the nonmagnetic case and the  $\sigma^*$  bands in the ferromagnetic and antiferromagnetic cases. The energy values concerning the oxygen-vacancy formation from  $\text{SrFeO}_3$  to  $\text{SrFeO}_{2.875}$  have been deduced with the correction of the  $\text{O}_2$  overbinding error and the consideration of the oxygen partial pressure and the temperature.

### 1. Introduction

$\text{SrFeO}_{3-\delta}$  species have been investigated extensively, due to their interesting electronic, magnetic, and transport properties. Their flexible accommodation of highly mobile oxygen vacancies, in combination with high electronic conductivity, makes them appealing for applications such as electrodes of solid oxide fuel cells, electrochemical catalysts, membranes for oxygen separation, and gas sensors. At low temperatures (below certain composition-dependent transition temperatures), the oxygen-vacancy ordered phases have been observed as the  $\text{Sr}_n\text{Fe}_n\text{O}_{3n-1}$  series, where  $n = 1, 2, 4, 8$ , and  $\infty$  after updated by the report of  $\text{SrFeO}_2$ .<sup>1</sup> However, at elevated temperatures the cubic perovskite structure remains up to  $\delta = 0.5$  with disordered oxygen vacancies, and corresponding research is essential to the high-temperature applications.

Although the perfect  $\text{SrFeO}_3$  has been explored theoretically at various levels, the computational investigation on the defective  $\text{SrFeO}_{3-\delta}$  with  $\delta \neq 0$  seems relatively limited. Koslowski<sup>2</sup> has analyzed the electronic structures of the cubic nonmagnetic (NM)  $\text{SrFeO}_{3-\delta}$  with  $0 \leq \delta \leq 0.5$ , using simple but physically transparent models. It is found that with increasing

$\delta$ , the density of states (DOS) at the Fermi level ( $E_F$ ) decreases, and the localization of eigenfunctions at  $E_F$  increases. Meanwhile, the obtained  $E_F$  lies at the top of the  $\sigma^*$  band, independent of  $\delta$ , which has been taken as a discrepancy from the previous hypothesis of Goodenough.<sup>3</sup> Shein et al.<sup>4</sup> have calculated the electronic properties of the cubic ferromagnetic (FM)  $\text{SrFeO}_{2.875}$  at the generalized gradient approximation (GGA) level based on the density functional theory (DFT) and obtained the vacancy formation energy of 2.90 eV.

The present work aims to analyze systematically the structural and electronic properties of the cubic  $\text{SrFeO}_{2.875}$  at the GGA +  $U$  level, considering the NM, FM, and G-type antiferromagnetic (AFM) configurations. Since such a level might not be suitable for metallic phases,<sup>5</sup> the pure GGA level is adopted as well to facilitate comparison. In order to evaluate the influence of oxygen-vacancy formation, and to deduce the formation energy, equivalent calculations are performed on the  $\text{SrFeO}_3$  counterparts. The thermodynamic corrections are provided to account for the oxygen partial pressure and temperature.

### 2. Computational Details

The adopted atomic positions for the NM, FM and AFM  $\text{SrFeO}_3$  are illustrated in Figure 1 (a) to (c), respectively. The experimental lattice parameter  $a = 3.869 \text{ \AA}$  was

\* Corresponding author phone: +86-10-62650558; fax: +86-10-62536108; e-mail: wlhuang@home.ipe.ac.cn.

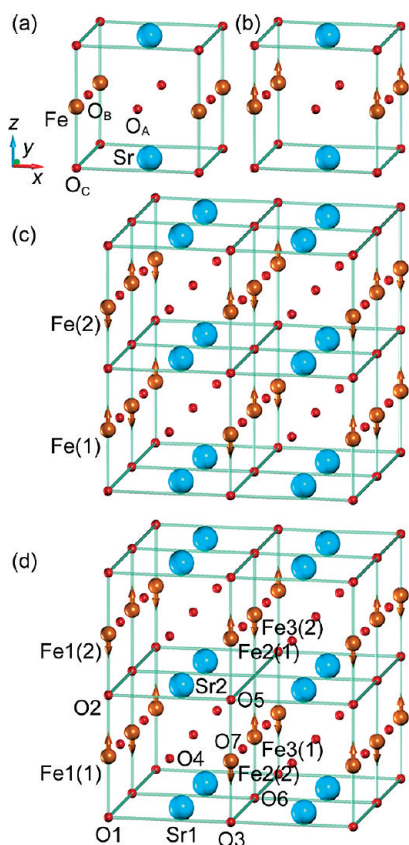


**Figure 1.** The adopted (a) NM and (b) FM  $\text{SrFeO}_3$  unit cells and AFM (c)  $(\text{SrFeO}_3)_8$  and (d) unrelaxed  $(\text{SrFeO}_{2.875})_8$  supercells. The arrows show the majority-spin orientations of the Fe atoms in the spin-polarized cases.

employed in the present work as in the literature.<sup>6</sup> As for the AFM  $\text{SrFeO}_3$ , we utilized a  $(\text{SrFeO}_3)_8$  supercell rather than the body-centered tetragonal primitive cell  $(\text{SrFeO}_3)_2$  (as adopted by Jaya et al.<sup>6</sup>) so as to decompose the Fe  $3d$  orbitals into comparative components, and in light of the majority-spin directions, the Fe atoms are divided into Fe(1) and Fe(2) types. The  $\text{SrFeO}_{2.875}$  is modeled via a  $(\text{SrFeO}_{2.875})_8$  supercell, built by removing the central oxygen atom of the  $(\text{SrFeO}_3)_8$  supercell and then shrinking the lattice constant from  $2 a$  to  $2 a_p$ , where  $a_p = 3.864 \text{ \AA}$  as treated in the literature.<sup>1</sup> According to the coordination environments and distances from the oxygen vacancy, Fe, Sr, and O atoms are classified into three (Fe1 to Fe3), two (Sr1 and Sr2), and seven (O1 to O7) kinds, respectively. In the AFM  $(\text{SrFeO}_{2.875})_8$  supercell, as shown in Figure 1 (d), each type of Fe atom can be distinguished further based on their majority-spin orientations, e.g., Fe1(1) or Fe1(2). To manifest the two different computational levels, the cases corresponding to the pure GGA level are labeled as NM1, FM1 and AFM1, while those at the GGA +  $U$  level are denoted by NM2, FM2, and AFM2.

Calculations were conducted via the plane-wave pseudopotential (PW-PP) DFT method as implemented in the Quantum-ESPRESSO package.<sup>7</sup> The Perdew-Burke-Ernzerhof (PBE)<sup>8</sup> GGA was employed for the exchange-correlation functional. Ultrasoft pseudopotentials (US-PPs) were used, where  $3d$  and  $4s$  states were considered for Fe with 8 e,  $4s$ ,  $4p$ ,  $4d$ ,  $5s$ , and  $5p$  states for Sr with 10 e, and  $2s$  and  $2p$  states for O with 6 e. All the pseudopotentials were generated

**Table 1.** Displacements ( $\text{\AA}$ ) of the Atoms in  $\text{SrFeO}_{2.875}$  Due to Relaxation

	NM1	NM2	FM1	FM2	AFM1	AFM2
Fe1	0.015	0.004	0.013	0.015	0.012	0.008
Fe2	0.022	0.020	0.023	0.022	0.021	0.016
Fe3	0.191	0.204	0.080	0.048	0.074	0.058
Sr1	0.101	0.101	0.040	0.031	0.028	0.036
Sr2	0.061	0.072	0.093	0.093	0.060	0.070
O1	0.000	0.000	0.000	0.000	$\approx 0.000$	$\approx 0.000$
O2	0.000	0.000	0.000	0.000	$\approx 0.000$	$\approx 0.000$
O3	0.000	0.000	0.000	0.000	$\approx 0.000$	$\approx 0.000$
O4	0.031	0.023	0.011	0.017	0.029	0.034
O5	0.000	0.000	0.000	0.000	$\approx 0.000$	$\approx 0.000$
O6	0.000	0.000	0.000	0.000	$\approx 0.000$	$\approx 0.000$
O7	0.180	0.183	0.144	0.174	0.209	0.218

with scalar-relativistic calculations, and nonlinear core corrections (NLCC) were included in the pseudopotentials of Fe and Sr. Within the GGA +  $U$  scheme, the value of  $U = 4.3 \text{ eV}$  was applied to the Fe species.

The kinetic energy cutoffs of 40 and 500 Ry were employed for the smooth part of the electronic wave functions and the augmented electron density respectively to achieve a total-energy difference below 1 meV/atom, accompanied by a Monkhorst-Pack<sup>9</sup>  $k$ -point grid (centered at the  $\Gamma$  point) of  $8 \times 8 \times 8$  for  $\text{SrFeO}_3$  and  $4 \times 4 \times 4$  for  $(\text{SrFeO}_3)_8$  and  $(\text{SrFeO}_{2.875})_8$ . The cold smearing<sup>10</sup> of 0.01 Ry was selected, and all the atomic positions in  $(\text{SrFeO}_{2.875})_8$  were relaxed until all components of the residual forces were smaller than  $0.026 \text{ eV}/\text{\AA}$  via the Broyden, Fletcher, Goldfarb, Shanno (BFGS)-based method.<sup>11</sup> The tetrahedron method<sup>12</sup> was exploited to calculate the DOS, and the atomic populations were analyzed using both the Löwdin<sup>13</sup> (included in the Quantum-ESPRESSO package<sup>7</sup>) and the Bader<sup>14</sup> (by means of the program developed by Henkelman et al.<sup>15</sup>) methods.

In order to figure out the oxygen-vacancy formation energy during the transformation from  $\text{SrFeO}_3$  to  $\text{SrFeO}_{2.875}$ , the triplet  $\text{O}_2$  was relaxed, and subsequent calculations were performed in a  $10 \text{ \AA}$  cubic box, as employed by Choi et al.<sup>16</sup> with a  $k$  point at the  $\Gamma$ . The kinetic energy cutoffs of 80 and 500 Ry were chosen for wave functions and charge density, respectively, to ensure a total-energy difference below 2 meV/atom.

To determine the reduction limit of the  $\text{O}_2$  partial pressure, the total energy values of Fe and  $\text{SrO}$  were computed additionally with the experimental lattice parameters,<sup>17</sup> using the same cutoffs as for  $\text{SrFeO}_3$ , and the  $k$  points were sampled with a separation about  $0.04 \text{ 1/\AA}$  in each of the three reciprocal lattice directions.

### 3. Results and Discussion

**3.1. Atomic Positions and Populations.** As explicated in Table 1, the relaxation generally leads to apparent changes in the positions of the nearest-neighbor (NN) (Fe3, Sr2, and O7) atoms of the oxygen vacancy in  $\text{SrFeO}_{2.875}$ , but many atoms beyond experience certain influences as well, especially Sr1 atoms whose displacements (away from the vacancy equally along the  $x$ - and  $y$ -axes, and additional variation also appears along the  $z$ -axis for the AFM cases)

are even more sizable than Sr2 in the NM cases. All the Fe1 and Fe2 atoms move along the  $z$ -axis. The Fe2 atoms in all cases and the Fe1 atoms in the NM cases approach the vacancy, while the Fe1 atoms in the FM and AFM cases are displaced away from the vacancy. The O4 atoms shift away from (or toward) the vacancy along the  $x$ -axis in the FM (or NM and AFM) cases and away from the vacancy along the  $z$ -axis in all the cases, and the displacements along the  $z$ -axis are more significant than along the  $x$ -axis. In comparison with the FM results calculated using the atomic orbitals as basis sets,<sup>4</sup> the present work offers the same trend and comparable displacement values for the NN atoms. The eight NN O7 atoms relax toward the vacancy (basically along the  $z$ -axis), whereas the two NN Fe3 and four NN Sr2 atoms retreat from the vacancy (along the  $z$ -axis for the former and equally along the  $x$ -axis and  $y$ -axis for the latter except for the AFM cases where slight shifts along the  $z$ -axis have also occurred). Such results can be interpreted based mostly on the electrostatic interactions within the ionic pictures. According to the simple empirical model in the Kröger-Vink notation,  $O \rightarrow V_O^{+} + 1/2 O_2(g) + 2 e'$ , the oxygen vacancy is positively charged and thus attracts the negative oxygen and repulses positive Fe and Sr ions in the lattice. Similar phenomena have been encountered in the literature, e.g., the oxygen vacancy repulses the neighboring Ti atoms, and the Sr or Ti vacancy repels the neighboring oxygen atoms in the defective SrTiO<sub>3</sub>.<sup>18</sup> The absolute values of the displacements are in the order of O7 > Sr2  $\approx$  Fe3 for the FM and AFM configurations and of Fe3 > O7 > Sr2 in the NM cases. These findings can be roughly correlated with the corresponding charges and interatomic distances. Neglecting the charge transfer induced by the vacancy formation, Fe3 exhibits the highest nominal valence (+4), along with the shortest distance from the vacant site ( $1/2 a_p$ , compared with  $\sqrt{2}/2 a_p$  for those of Sr2 or O7 before relaxation), and the largest displacements can be expected. Reduction due to the charge transfer (described below) weakens the electrostatic interaction between Fe3 or Sr2 and the vacancy and yields their smaller displacements, while reverse results might be anticipated for the negatively charged O7.

To elucidate the vacancy-incurred charge transfer, we analyzed the atomic populations in both SrFeO<sub>3</sub> and Sr-FeO<sub>2.875</sub>. The Löwdin results of SrFeO<sub>3</sub> and SrFeO<sub>2.875</sub> are provided in Table 2. It is obvious that the vacancy transfers charges principally to the NN atoms, and the order of transfer amount is generally Fe3 > Sr2  $\approx$  O7. To make a crosscheck on the tendency, the Bader analyses were complemented, as in Table 3, and coherent tendencies can be observed.

A comparable amount of charge transfer to Fe3 shortens its displacement in the NM cases less than in the FM and AFM cases, owing to the relatively larger dispersivity of the 3d orbitals (that accept the charges) in the NM cases, and the Fe3 shows still greater displacements than O7 and Sr2 in the NM cases. The longer displacements of O7 than Sr2 might be ascribed qualitatively to the larger charge transfer to Sr2 as well as the steric factor: the smaller size of oxygen and more space and thus more feasibility to approach the vacancy.

**Table 2.** Löwdin Populations (e) of the Atoms in SrFeO<sub>3</sub> and SrFeO<sub>2.875</sub>

		NM1	NM2	FM1	FM2	AFM1	AFM2
<i>a</i>	Fe	6.71	6.81	6.45	6.31	6.45	6.36
	Sr	9.86	9.85	9.90	9.93	9.90	9.92
	O	6.45	6.42	6.51	6.55	6.51	6.54
<i>b</i>	Fe1	6.68	6.81	6.47	6.31	6.43	6.35
	Fe2	6.72	6.82	6.45	6.28	6.42	6.33
	Fe3	6.85	6.87	6.52	6.38	6.53	6.47
	Sr1	9.84	9.83	9.88	9.90	9.88	9.90
	Sr2	9.88	9.88	9.93	9.96	9.93	9.95
	O1	6.44	6.44	6.51	6.55	6.51	6.52
	O2	6.42	6.44	6.51	6.55	6.51	6.52
	O3	6.46	6.45	6.54	6.59	6.55	6.58
<i>c</i>	O4	6.44	6.42	6.52	6.56	6.53	6.54
	O5	6.44	6.41	6.52	6.55	6.52	6.55
	O6	6.40	6.33	6.50	6.63	6.55	6.58
	O7	6.48	6.45	6.54	6.57	6.54	6.56

<sup>a</sup> SrFeO<sub>3</sub>. <sup>b</sup> SrFeO<sub>2.875</sub>.

**Table 3.** Bader Populations (e) of the Atoms in SrFeO<sub>3</sub> and SrFeO<sub>2.875</sub>

		NM1	NM2	FM1	FM2	AFM1	AFM2
<i>a</i>	Fe	6.21	6.29	6.09	6.02	6.08	6.05
	Sr	8.37	8.37	8.38	8.39	8.38	8.39
	O	7.14	7.12	7.18	7.20	7.18	7.19
<i>b</i>	Fe1	6.21	6.29	6.09	5.99	6.04	6.09
	Fe2	6.22	6.31	6.13	6.03	6.09	6.05
	Fe3	6.39	6.37	6.25	6.19	6.21	6.21
	Sr1	8.41	8.41	8.39	8.40	8.40	8.41
	Sr2	8.41	8.41	8.42	8.42	8.42	8.42
	O1	7.19	7.19	7.19	7.23	7.20	7.17
	O2	7.20	7.18	7.22	7.25	7.21	7.24
	O3	7.17	7.16	7.22	7.24	7.23	7.25
	O4	7.16	7.14	7.22	7.24	7.21	7.21
	O5	7.17	7.12	7.22	7.21	7.23	7.20
	O6	7.03	7.06	7.13	7.21	7.18	7.17
	O7	7.15	7.13	7.18	7.21	7.21	7.21

<sup>a</sup> SrFeO<sub>3</sub>. <sup>b</sup> SrFeO<sub>2.875</sub>.

Introduction of the Hubbard  $U$  term enlarges the displacements of O7 in all cases, Fe3 in the NM case, and Sr2 in the NM and AFM cases, while it reduces those of Fe3 in the FM and AFM cases. Electrostatic analysis can offer a reasonable explanation again. Take the displacements of Fe3 as an example. In comparison with the GGA method, the GGA +  $U$  level generates smaller occupancy difference between Fe1 and Fe3 in the NM case and larger ones in the FM and AFM cases. Assuming that the Fe1 atoms receive no influence and charge transfer from the vacancy formation, the above results mean that the charge transfer to Fe3 is smaller in the NM case, and larger in the FM and AFM cases, when the  $U$  term is introduced. This is in accord with the displacement changes.

To describe the charge distribution among the Fe 3d orbitals, the relevant Löwdin populations are listed in Table 4. Referring to SrFeO<sub>3</sub>, the Fe3 atoms in NM SrFeO<sub>2.875</sub> accept electrons largely on the  $3d_z^2$  or  $3d_{x^2-y^2}$  orbital. It is also evident that the  $3d_{xz}$ ,  $3d_{yz}$ , and  $3d_{xy}$  orbitals contribute more than the  $3d_z^2$  and  $3d_{x^2-y^2}$  ones to the Fe magnetic moments in the FM and AFM cases. The oxygen vacancy enhances the spin polarization on the Fe3  $3d_z^2$  orbital and weakens that on the Fe3  $3d_{x^2-y^2}$  orbital, while the Fe2 atoms

**Table 4.** Löwdin Populations (e) of the Fe or Fe(1) 3d Orbitals in Different Cases

	$z^2$		$xz$		$yz$		$x^2 - y^2$		$xy$		total	
	$\uparrow$	$\downarrow$	$\uparrow$	$\downarrow$	$\uparrow$	$\downarrow$	$\uparrow$	$\downarrow$	$\uparrow$	$\downarrow$	$\uparrow$	$\downarrow$
NM1 <sup>a</sup>	0.95		1.52		1.52		0.95		1.52		6.45	
NM2 <sup>a</sup>	0.79		1.66		1.66		0.79		1.66		6.55	
FM1 <sup>a</sup>	0.77	0.34	1.00	0.32	1.00	0.32	0.77	0.34	1.00	0.32	4.53	1.65
FM2 <sup>a</sup>	0.88	0.36	0.99	0.20	0.99	0.20	0.88	0.36	0.99	0.20	4.73	1.31
AFM1 <sup>b</sup>	0.78	0.46	0.98	0.26	0.98	0.26	0.78	0.46	0.98	0.26	4.50	1.68
AFM2 <sup>b</sup>	0.86	0.46	0.99	0.16	0.99	0.16	0.86	0.46	0.99	0.16	4.68	1.41
NM1 <sup>c</sup>	0.92		1.54		1.54		0.91		1.52		6.43	
NM1 <sup>d</sup>	0.92		1.50		1.58		0.94		1.53		6.47	
NM1 <sup>e</sup>	1.12		1.49		1.49		0.96		1.54		6.60	
NM2 <sup>c</sup>	0.75		1.70		1.70		0.74		1.68		6.56	
NM2 <sup>d</sup>	0.74		1.60		1.79		0.76		1.68		6.57	
NM2 <sup>e</sup>	0.78		1.66		1.66		0.88		1.63		6.61	
FM1 <sup>c</sup>	0.79	0.34	0.99	0.32	0.99	0.32	0.77	0.35	0.99	0.34	4.54	1.67
FM1 <sup>d</sup>	0.81	0.32	0.99	0.29	0.99	0.32	0.86	0.31	0.99	0.29	4.65	1.53
FM1 <sup>e</sup>	0.86	0.31	0.99	0.35	0.99	0.35	0.70	0.39	0.99	0.32	4.53	1.72
FM2 <sup>c</sup>	0.89	0.35	0.99	0.19	0.99	0.19	0.88	0.36	0.99	0.19	4.75	1.28
FM2 <sup>d</sup>	0.90	0.34	0.99	0.19	0.99	0.15	0.93	0.33	0.99	0.18	4.81	1.19
FM2 <sup>e</sup>	0.95	0.29	0.99	0.22	0.99	0.22	0.81	0.41	0.99	0.22	4.74	1.36
AFM1 <sup>f</sup>	0.79	0.45	0.99	0.24	0.99	0.24	0.80	0.44	0.99	0.24	4.55	1.61
AFM1 <sup>g</sup>	0.81	0.41	0.99	0.24	0.99	0.23	0.88	0.38	0.99	0.23	4.66	1.50
AFM1 <sup>h</sup>	0.92	0.41	0.98	0.31	0.98	0.31	0.58	0.49	0.99	0.28	4.46	1.80
AFM2 <sup>f</sup>	0.86	0.46	0.99	0.16	0.99	0.16	0.87	0.46	0.99	0.16	4.69	1.39
AFM2 <sup>g</sup>	0.89	0.43	0.99	0.16	0.99	0.14	0.93	0.38	0.99	0.15	4.80	1.26
AFM2 <sup>h</sup>	0.95	0.42	0.99	0.22	0.99	0.22	0.68	0.51	0.99	0.21	4.60	1.59

<sup>a</sup> Fe in SrFeO<sub>3</sub>. <sup>b</sup> Fe(1) in SrFeO<sub>3</sub>. <sup>c</sup> Fe1 in SrFeO<sub>2.875</sub>. <sup>d</sup> Fe2 in SrFeO<sub>2.875</sub>. <sup>e</sup> Fe3 in SrFeO<sub>2.875</sub>. <sup>f</sup> Fe1(1) in SrFeO<sub>2.875</sub>. <sup>g</sup> Fe2(1) in SrFeO<sub>2.875</sub>. <sup>h</sup> Fe3(1) in SrFeO<sub>2.875</sub>.

show a vacancy-induced increase in the magnetic moments of almost all five 3d orbitals.

**3.2. Electronic Band Structures.** Regardless of the reduction from SrFeO<sub>3</sub> to SrFeO<sub>2.875</sub>, the magnetic patterns (NM, FM, or AFM), and the change in computational level from pure GGA to GGA + *U*, the band sequence remains unchanged: Sr 4s, O 2s, and Sr 4p form the lowest three occupied bands sequentially with increasing energy, the hybridization of O 2p and Fe 3d exists around  $E_F$ , and Sr 4d, Fe 3s, Sr 5s, and Sr 5p contribute to the bands of higher energy. Figures 2–4 depict the total and partial density of states (PDOS) of the species in NM, FM, and AFM configurations, respectively, calculated within the GGA + *U* scheme. In the displayed energy range, the Fe 4s states exhibit negligible density though plotted, and the trivial contribution of Sr 5s and 5p has been omitted. The (P)DOS peaks in SrFeO<sub>2.875</sub> are generally lower but wider than their counterparts in SrFeO<sub>3</sub>, and some peaks have decomposed, due to the lowering of the symmetry.

Based on simple models, Koslowski has reported the decreasing DOS at  $E_F$  with increasing  $\delta$  for NM SrFeO<sub>3- $\delta$</sub> . This trend has not been reproduced in our NM1 cases (8.77 and 9.02 states/(eV fu) for SrFeO<sub>3</sub> and SrFeO<sub>2.875</sub>, respectively) but appears somewhat in the NM2 cases (7.63 and 7.56 states/(eV fu) for SrFeO<sub>3</sub> and SrFeO<sub>2.875</sub>, respectively), considering  $\delta = 0$  and 0.125. By the way, Jaya et al. has given a value of 11.94 states/(eV fu) for NM SrFeO<sub>3</sub>.<sup>6</sup>

The obtained values of the total magnetic moment are 3.61 and 4.05  $\mu_B$ /fu (formula) for FM1 and FM2 SrFeO<sub>3</sub>, respectively, whereas the counterparts for SrFeO<sub>2.875</sub> are 3.79 and 4.25  $\mu_B$ /fu correspondingly. The absolute magnetic moment of AFM1 SrFeO<sub>3</sub> is 3.13  $\mu_B$ /fu, and that of AFM2 SrFeO<sub>3</sub> is 3.56  $\mu_B$ /fu. In contrast, the AFM1 and AFM2 cases of SrFeO<sub>2.875</sub> yield 3.36 and 3.70  $\mu_B$ /fu, respectively. It is

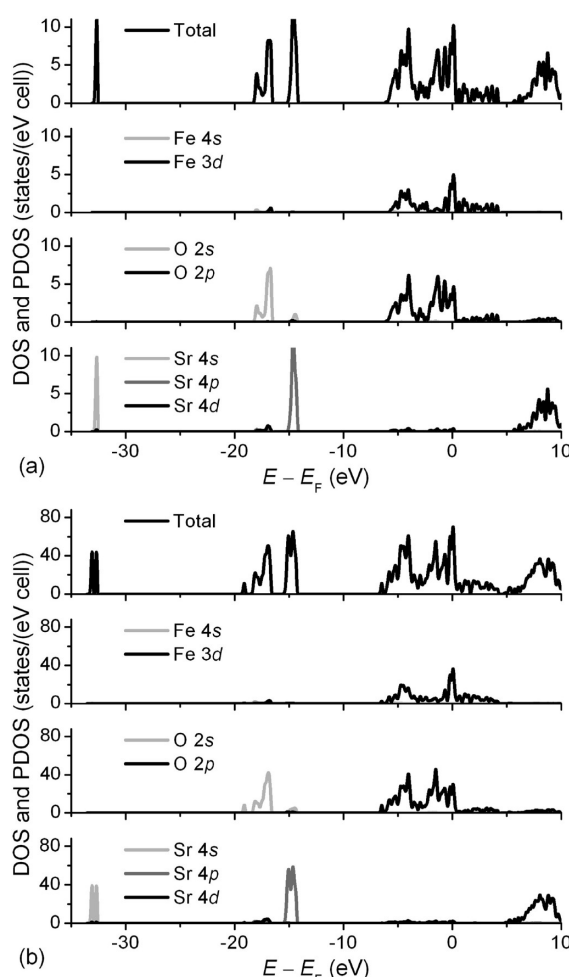


**Figure 2.** Total and partial DOS of NM2 (a) SrFeO<sub>3</sub> and (b) (SrFeO<sub>2.875</sub>)<sub>8</sub>.

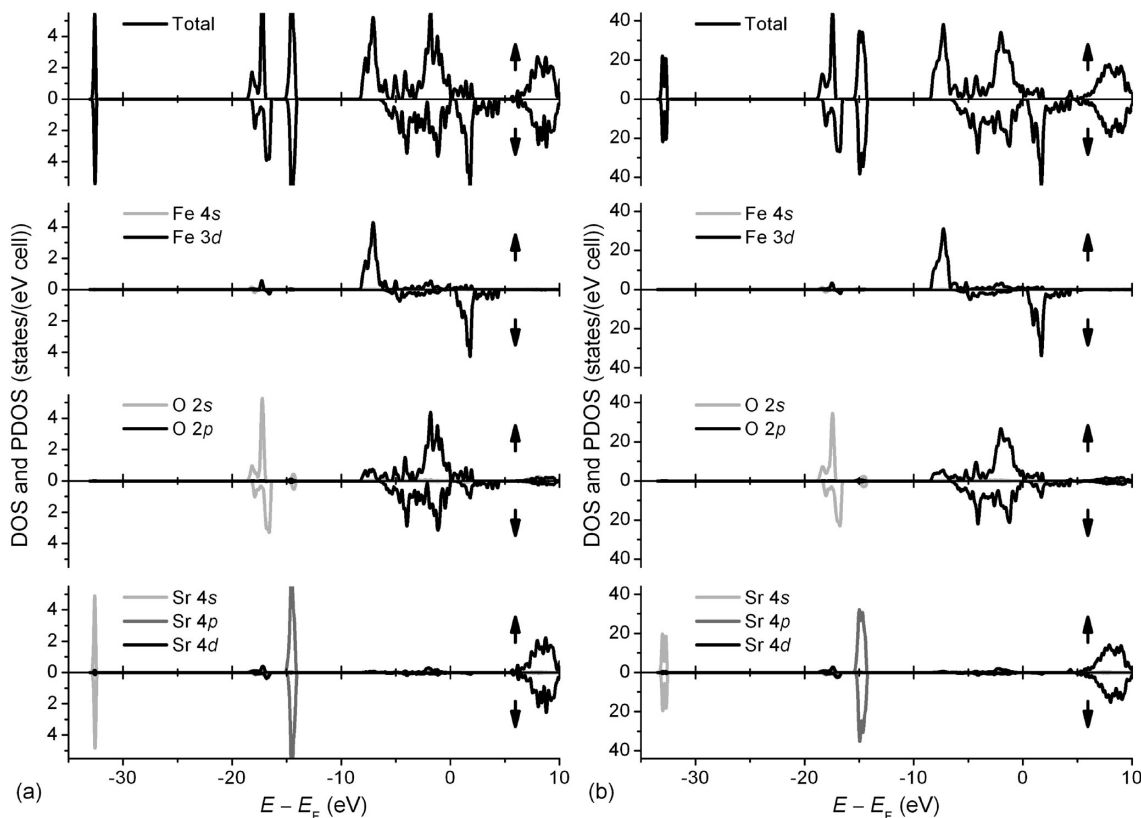


**Figure 3.** Total and partial DOS of FM2 (a)  $\text{SrFeO}_3$  and (b)  $(\text{SrFeO}_{2.875})_8$ .

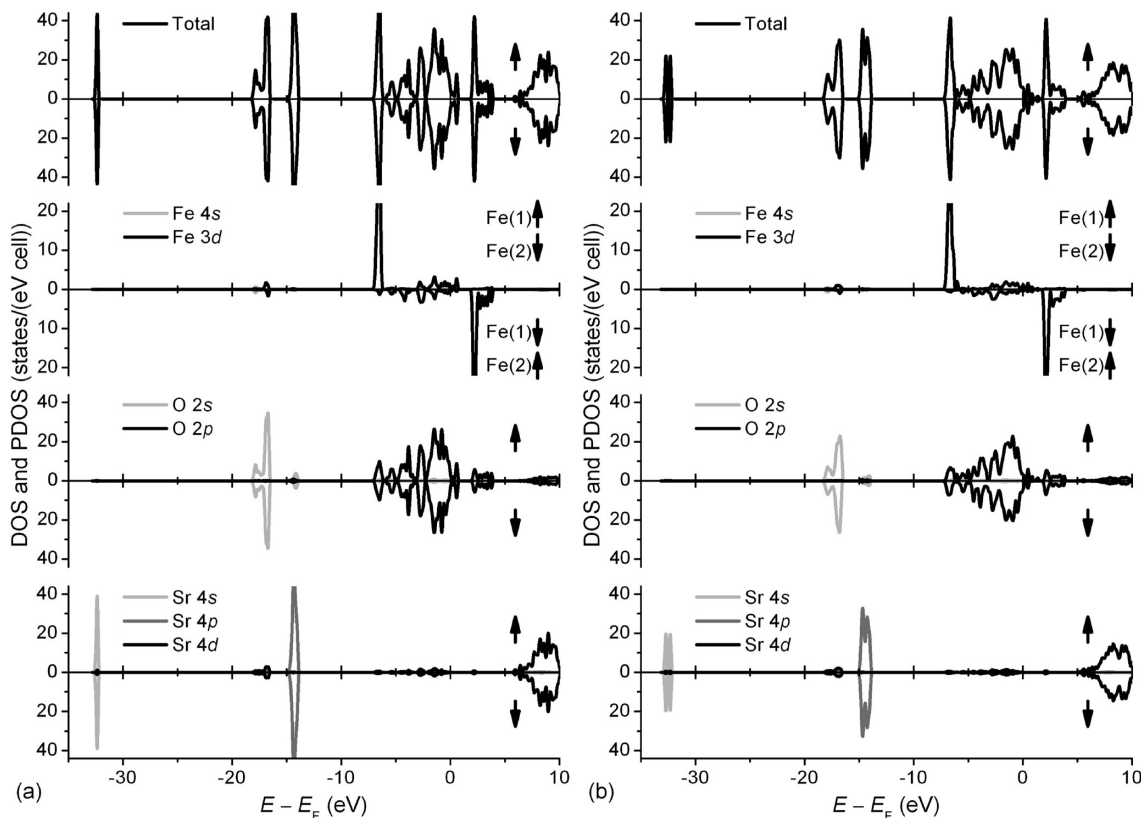
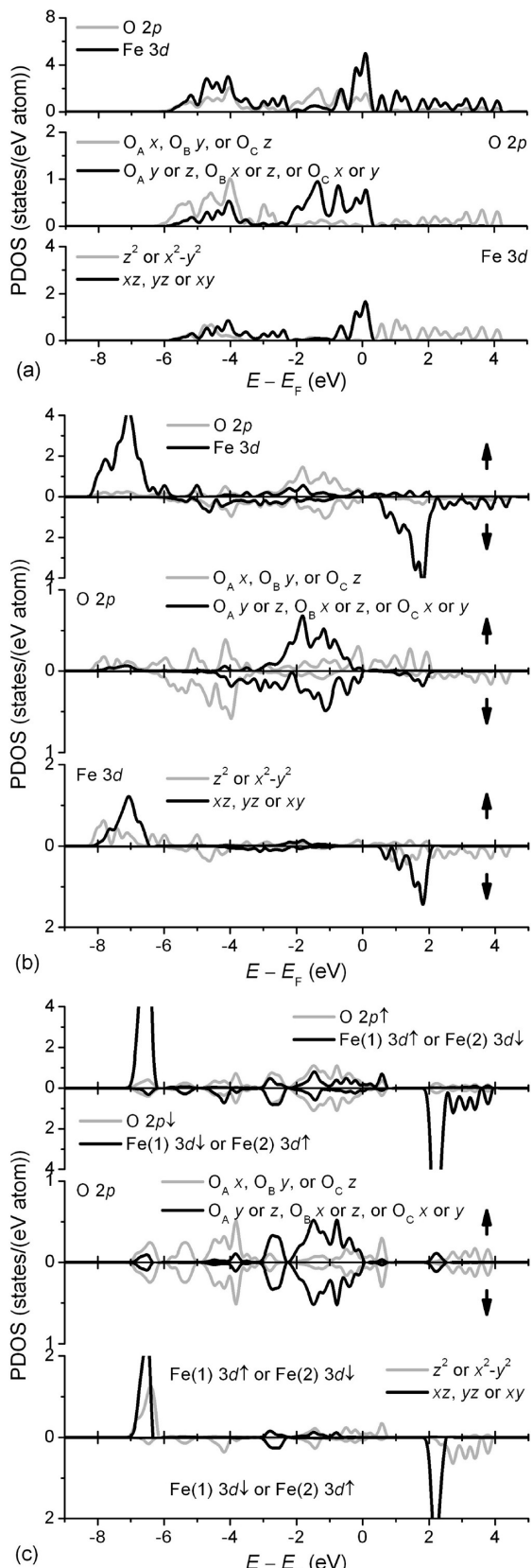


**Figure 4.** Total and partial DOS of AFM2 (a)  $(\text{SrFeO}_3)_8$  and (b)  $(\text{SrFeO}_{2.875})_8$ .

obvious that both the Hubbard  $U$  term and the oxygen vacancy have improved the magnetic moments.

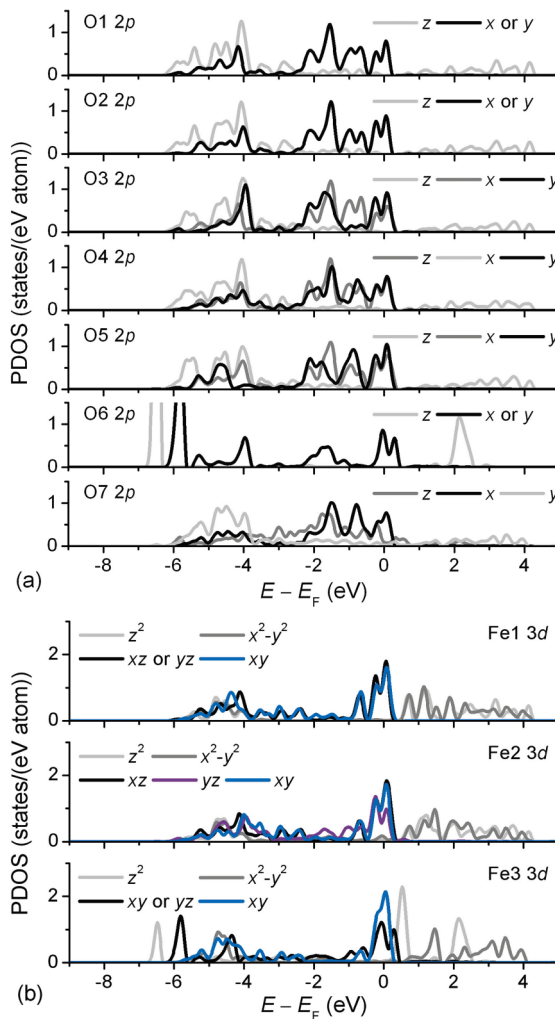
In order to reveal the bonding characteristics, we provide the components of O 2p and Fe 3d orbitals and their overlapping. The GGA +  $U$  results for  $\text{SrFeO}_3$  are given in

Figure 5. For the NM2 case, the  $\sigma$  bonding is within  $-5.7 \sim -3.6$  eV, the  $\pi$  bonding covers  $-5.6 \sim -2.3$  eV, the  $\pi^*$  antibonding emerges in the energy range of  $-0.8 \sim 0.3$  eV, and the  $\sigma^*$  antibonding is apparent in  $0.4 \sim 4.3$  eV. The observed crystal field splitting is about 1.2 eV, and the Fermi



**Figure 5.** Overlap between O 2p and Fe 3d orbitals in (a) NM2, (b) FM2, and (c) AFM2 SrFeO<sub>3</sub>.

level is situated in the  $\pi^*$  antibonding region, which is coincident with the result of Matar.<sup>19</sup> In the FM2 case, the majority spin channel shows the  $\sigma$ ,  $\pi$  bonding and  $\pi^*$ ,  $\sigma^*$  antibonding within  $-8.2$  to  $-5.8$ ,  $-8.0$  to  $-6.5$ ,  $-2.5$  to  $-1.2$ , and  $-0.3$  to  $-2.1$  eV, respectively, and for the minority



**Figure 6.** The components of (a) O 2p and (b) Fe 3d PDOS in NM2 SrFeO<sub>2.875</sub>.

spin channel, the observable regions are  $-6.0$  to  $-4.0$ ,  $-4.4$  to  $-0.8$ ,  $0.9$  to  $-2.1$ , and  $0.7$  to  $-4.5$  eV correspondingly, with the exchange splitting around 2.9 eV. The larger exchange splitting than the crystal field splitting favors the high-spin (HS) structure. Regarding the AFM2 case, the energy ranges concerning the  $\sigma$ ,  $\pi$  bonding and  $\pi^*$ ,  $\sigma^*$  antibonding are  $-7.0$  to  $-6.2$ ,  $-6.8$  to  $-6.4$ ,  $-3.0$  to  $-0.7$ , and  $-1.8$  to  $-0.7$  eV, respectively, for the Fe(1) majority spin part and  $-6.7$  to  $-4.0$ ,  $-3.0$  to  $-2.3$ ,  $2.0$  to  $-2.5$ , and  $2.2$  to  $-4.0$  eV for the Fe(1) minority spin one.

Figures 6–8 plot the PDOS of O 2p and Fe 3d orbitals in SrFeO<sub>2.875</sub> obtained within the GGA +  $U$  scheme. The oxygen vacancy has tailored the structural and electronic properties apparently, removing the orbital degeneracies. Referring to those in SrFeO<sub>3</sub>, the 2p (as well as 2s, not shown) orbitals of O6 and O7 exhibit the most significant difference. The  $\sigma$  bonding and  $\sigma^*$  antibonding between O6 2p and Fe3 3d becomes highly localized, and in the NM2 case such bonding might be the strongest among the O 2p–Fe 3d pairs, appearing within the lowest energy range. A half-metallic feature can be noticed in FM2 SrFeO<sub>2.875</sub>.

To further discern the states at  $E_F$ , the local DOS (LDOS) isosurfaces are presented in Figure 9, rendered via the XCrySDen code.<sup>20</sup> Associated with Figures 6–8, Figure 9 shows that the states at  $E_F$  correspond to the  $\pi^*$  antibonding

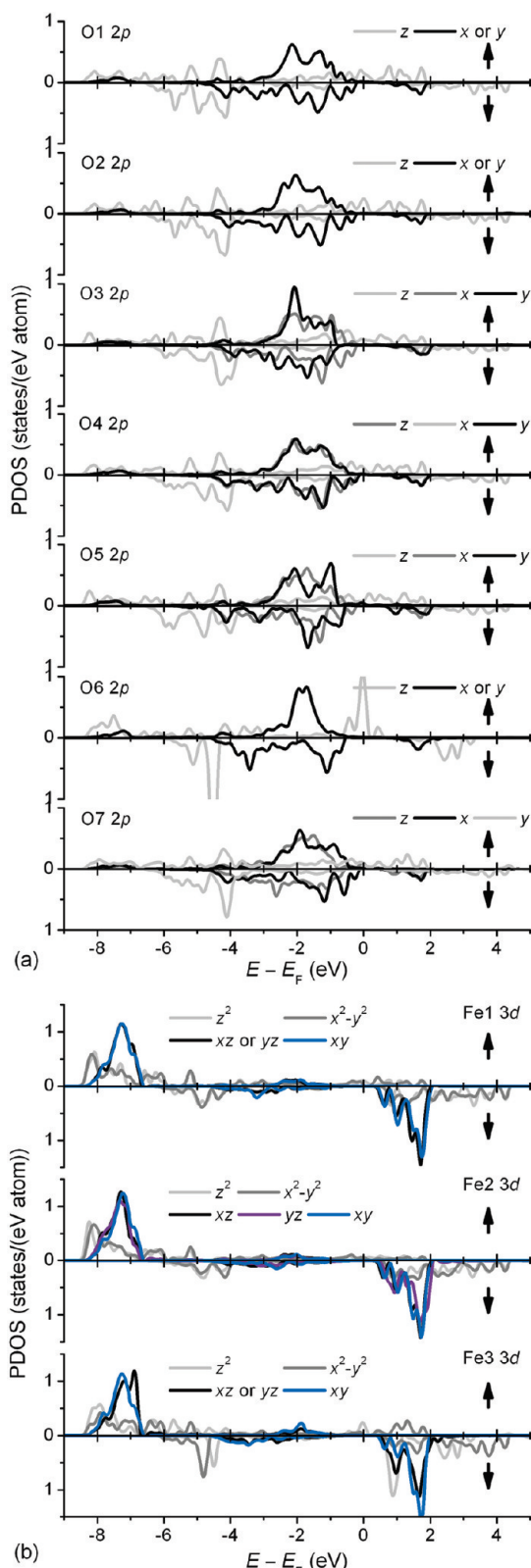


**Figure 7.** The components of (a) O 2p and (b) Fe 3d PDOS in FM2  $\text{SrFeO}_{2.875}$ .

for NM2  $\text{SrFeO}_3$  and  $\text{SrFeO}_{2.875}$ , and the  $\sigma^*$  antibonding in the spin-up channel for FM2  $\text{SrFeO}_3$  and  $\text{SrFeO}_{2.875}$ . The AFM2  $\text{SrFeO}_{2.875}$  displays the  $\sigma^*$  antibonding of the Fe1 and Fe2 3d orbitals with the 2p orbitals of adjacent oxygen atoms at  $E_F$ , while the local states of AFM2  $\text{SrFeO}_3$  at  $E_F$  manifest the nonbonding nature. Koslowski<sup>2</sup> has explored NM  $\text{Sr}$ -

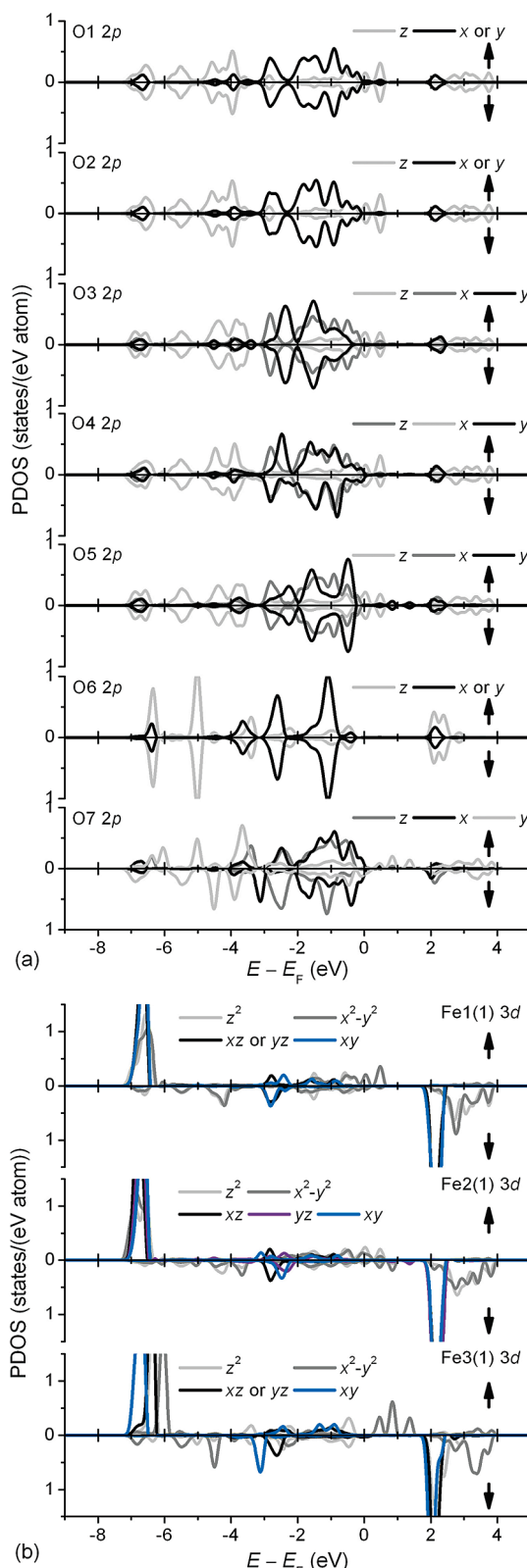


**Figure 8.** The components of (a) O 2p and (b) Fe 3d PDOS in AFM2  $\text{SrFeO}_{2.875}$ .

$\text{FeO}_{3-\delta}$  using simple models and found that the  $\sigma^*$  antibonding states arise at  $E_F$ , which is reckoned as a difference from Goodenough's hypothesis.<sup>3</sup> However, Goodenough has predicted the  $\pi^*$  antibonding states at  $E_F$  based on low-spin (LS)  $\text{Fe}^{4+}$ , expecting FM coupling. Concerning the NM pattern, the exchange splitting is neglected, and it is

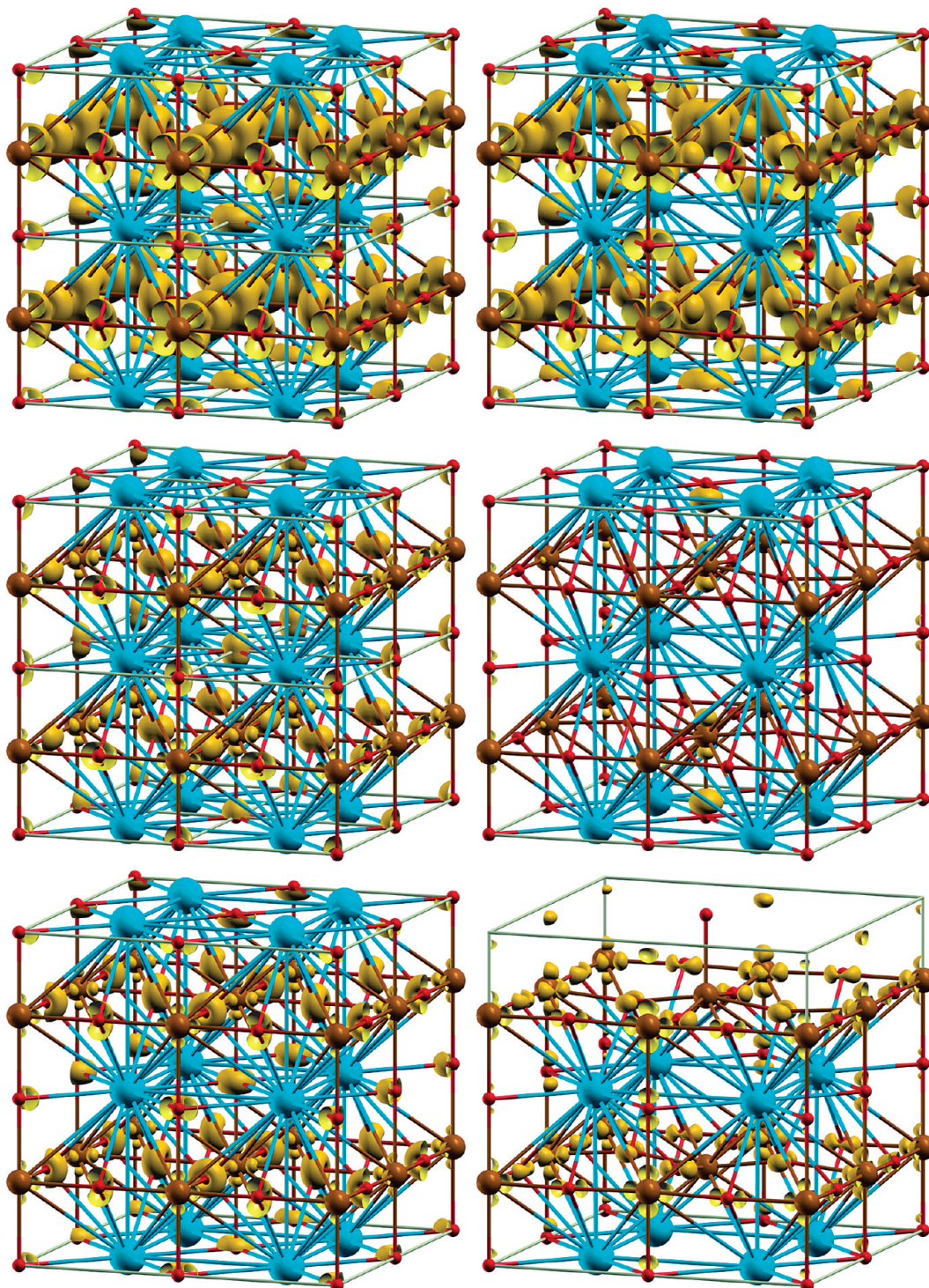


**Figure 9.** The local DOS isosurfaces at  $E_F$  of NM2 (top), FM2 (middle), and AFM2 (bottom)  $\text{SrFeO}_3$  (left) and  $\text{SrFeO}_{2.875}$  (right), rendered with an isovalue of 1.0.

reasonable that the crystal field makes the partially filled  $\pi^*$  orbitals and empty  $\sigma^*$  ones for  $\text{Fe}^{4+}$  ( $3d^4$ ). This is consistent with the results of Matar<sup>19</sup> and Jaya et al.<sup>6</sup> for  $\text{SrFeO}_3$ , and the partially filled  $\sigma^*$  band achieved by Koslowski might be ascribed to some deficiencies of the Anderson-Mott-Hubbard model or its approximation.<sup>2</sup> Once the spin polarization is incorporated, the HS configuration has been found favorable experimentally<sup>19</sup> and theoretically,<sup>6,19</sup> which offers the  $\sigma^*$  states at  $E_F$ . Based on the competitive crystal field splitting and exchange splitting, and the resultant magnetic moments,

the principal HS pattern is confirmed for both  $\text{SrFeO}_3$  and  $\text{SrFeO}_{2.875}$  in the present work.

On the basis of the theorem of Anderson,<sup>21</sup> the orbital localization is expectable in disordered systems. Koslowski<sup>2</sup> has discovered the increasing localization of states at  $E_F$  with  $\delta$  in  $\text{SrFeO}_{3-\delta}$ . Similarly, as depicted in Figure 9, a reduced number of states appear in  $\text{SrFeO}_{2.875}$  in comparison with  $\text{SrFeO}_3$ , signifying the vacancy-induced localization at  $E_F$ . The orbital localization might also be implicated in the larger magnetic moments of  $\text{SrFeO}_{2.875}$  configurations than those of  $\text{SrFeO}_3$ .

counterparts, for localized electrons might carry spontaneous atomic moments while collective electrons might not.<sup>3</sup>

**3.3. Vacancy Formation Energetics.** Congruent with the reports in the literature,<sup>19,22</sup> both the present GGA and GGA + *U* calculations fail to predict the experimentally identified AFM ground state of SrFeO<sub>3</sub>. At the GGA level, the FM SrFeO<sub>3</sub> was computed to be 1.308 and 0.235 eV/fu more stable than the NM and AFM patterns, respectively, while the values are 2.098 and 0.196 eV/fu with the GGA + *U* approach, respectively. In comparison, Matar<sup>19</sup> reported that the FM state is 0.224 eV/fu more stable than the AFM state, via both the LMTO-ASA (linear muffin tin orbital-atomic sphere approximation) and the ASW (augmented spherical wave) methods (where), and Shein et al.<sup>22</sup> gave a value of 0.262 eV/fu using the LSDA (local spin density approximation) + *U* formalism with *U* = 6.0 eV and the exchange parameter *J* = 0.6 eV.

For the triplet O<sub>2</sub>, we obtained the relaxed O–O bond length of 1.236 Å, and the calculated vibrational frequency of 1572.2 cm<sup>-1</sup>. These agree well with the results calculated under the GGA-PAW (projector augmented wave) scheme and the experimental values.<sup>16</sup>

Following the reduction reaction, 8 SrFeO<sub>3</sub> → (SrFeO<sub>2.875</sub>)<sub>8</sub> + 1/2 O<sub>2</sub> (g), at the GGA level, the oxygen-vacancy formation energy is evaluated as

$$E_{\text{vf1}} = E((\text{SrFeO}_{2.875})_8)^{\text{GGA}} + 1/2E(\text{O}_2)^{\text{GGA}} - 8E(\text{SrFeO}_3)^{\text{GGA}} \quad (1)$$

where  $E(\text{O}_2)^{\text{GGA}}$  is the total energy of the triplet O<sub>2</sub>, while  $E((\text{SrFeO}_{2.875})_8)^{\text{GGA}}$  and  $E(\text{SrFeO}_3)^{\text{GGA}}$  are the total energy values of (SrFeO<sub>2.875</sub>)<sub>8</sub> and SrFeO<sub>3</sub> at this level, respectively. We obtain the  $E_{\text{vf1}}$  values of 0.35, 1.51, and 0.92 eV for the AFM, FM, and NM cases correspondingly. By comparison, Shein et al.<sup>4</sup> have reported that a value of 2.90 eV for the FM case, using the GGA approach as well, but Troullier-Martins norm-conserving pseudopotentials, the atomic orbitals basis sets, Sr 5s<sup>2</sup> p<sup>6</sup> 4d<sup>0</sup> configuration (8 *e*), and a value of 3.7054 Å for both *a* in SrFeO<sub>3</sub> and *a*<sub>p</sub> in (SrFeO<sub>2.875</sub>)<sub>8</sub>.

It is known that the O<sub>2</sub> molecule is overbound within both the LDA and GGA frameworks (the experimental binding energy of O<sub>2</sub> is about –5.23 eV,<sup>23</sup> in comparison with the GGA value<sup>5,24</sup> around –5.99 or –6.02 eV), which might cause an underestimate for the O-vacancy formation energy. By fitting the calculated formation energy of nontransition metal oxides from metals and O<sub>2</sub>, and comparing with the experimental formation enthalpy values, Wang et al.<sup>5</sup> derived a shift of 1.36 eV/O<sub>2</sub> (i.e., 0.68 eV per oxygen atom). This is larger than the binding energy difference and is surmised to be related with the electron transferring to (oxidation) or from (reduction) the oxygen 2p orbitals. Therefore, the correction in this aspect might suggest an addition of 0.68 eV to the calculated O-vacancy formation energy. In the other aspect, treating 3d metal states using LDA or GGA causes the well-known self-interaction error that incorrectly increases the energy of the reduced state (with more d electrons), thus overestimating the O-vacancy formation energy. It is found that the GGA + *U* scheme can remove this error for many systems to some extent via suitable *U*

values.<sup>5</sup> Since this error is opposite to and hence cancels the O<sub>2</sub> overbinding error to a certain degree, giving rise to better agreement with experiments, it is better to correct or uncorrect these two errors simultaneously. However, the above-mentioned cancellation is rather arbitrary, and the uncorrected results are essentially unreliable. Therefore, we evaluated further the corrected  $E_{\text{vf2}}$  values, using the GGA + *U* energetics and the 0.68 eV/O correction as expressed in

$$E_{\text{vf2}} = E((\text{SrFeO}_{2.875})_8)^{\text{GGA+U}} + 1/2E(\text{O}_2)^{\text{GGA}} - 8E(\text{SrFeO}_3)^{\text{GGA+U}} + 0.68 \text{ eV} \quad (2)$$

where  $E((\text{SrFeO}_{2.875})_8)^{\text{GGA+U}}$  and  $E(\text{SrFeO}_3)^{\text{GGA+U}}$  are the total energy values of (SrFeO<sub>2.875</sub>)<sub>8</sub> and SrFeO<sub>3</sub> achieved at the GGA + *U* level. The  $E_{\text{vf2}}$  results are 0.23, 1.35, and 1.32 eV for the AFM, FM, and NM structures, respectively.

Neglecting the *pV* (pressure *p* and the cell volume *V*) and vibrational contributions of the solid phases as in the literature,<sup>25–27</sup> the temperature and pressure dependence of  $E_{\text{vfi}}$  (*i* = 1 and 2) can be deduced simply by replacing the 1/2  $E(\text{O}_2)^{\text{GGA}}$  term in eqs 1 and 2 with the O chemical potential  $\mu_{\text{O}}(T, p(\text{O}_2))$  at the temperature *T* and the O<sub>2</sub> partial pressure *p(O<sub>2</sub>)*, and the resultant expressions are

$$E_{\text{vf1}}(T, p(\text{O}_2)) = E((\text{SrFeO}_{2.875})_8)^{\text{GGA}} + \mu_{\text{O}}(T, p(\text{O}_2)) - 8E(\text{SrFeO}_3)^{\text{GGA}} \quad (3)$$

$$E_{\text{vf2}}(T, p(\text{O}_2)) = E((\text{SrFeO}_{2.875})_8)^{\text{GGA+U}} + \mu_{\text{O}}(T, p(\text{O}_2)) - 8E(\text{SrFeO}_3)^{\text{GGA+U}} + 0.68 \text{ eV} \quad (4)$$

where  $\mu_{\text{O}}(T, p(\text{O}_2)) = 1/2 E(\text{O}_2)^{\text{GGA}} + 1/2 \Delta G(\Delta T, p^{\circ}(\text{O}_2), \text{O}_2) + 1/2 k_{\text{B}}T \ln(p(\text{O}_2)/p^{\circ}(\text{O}_2))$ ,  $k_{\text{B}}$  is the Boltzmann constant, and  $p^{\circ}(\text{O}_2)$  is the O<sub>2</sub> partial pressure at the standard state, i.e., 1 atm. Using the 1/2  $\Delta G(\Delta T, p^{\circ}(\text{O}_2), \text{O}_2)$  values tabulated by Reuter and Scheffler,<sup>25</sup> the  $E_{\text{vf1}}(T, 1 \text{ atm}) \sim T$  and  $E_{\text{vf1}}(700 \text{ K}, p(\text{O}_2)) \sim p(\text{O}_2)$  plots are provided in Figure 10. Different magnetic configurations have been presented here to facilitate mutual comparison; however, it should be noted that the *T<sub>N</sub>* of SrFeO<sub>3</sub> is around 130 or 134 K,<sup>6,19</sup> and in ordered SrFeO<sub>2.875</sub> the magnetic pattern was observed merely below about 85 K.<sup>28</sup> The lower and upper limits of *p(O<sub>2</sub>)* in Figure 10(b) were determined using the technique analogous to that in the literature for other systems.<sup>25,27</sup> The O-rich limit is defined as the point beyond which gas phase O starts to condense,<sup>25,26</sup> that is, let  $\mu_{\text{O}}(T, p(\text{O}_2)^{\text{max}}) = 1/2 E(\text{O}_2)^{\text{GGA}} + 1/2 \Delta G(\Delta T, p^{\circ}(\text{O}_2), \text{O}_2) + 1/2 k_{\text{B}}T \ln(p(\text{O}_2)^{\text{max}}/p^{\circ}(\text{O}_2)) = 1/2 E(\text{O}_2)^{\text{GGA}}$ , and obtain  $p(\text{O}_2)^{\text{max}} = 3.25 \times 10^{10}$  atm at *T* = 700 K. The O-poor limit is determined considering the coexistence of NM SrFeO<sub>3</sub> (the FM and AFM cases give much lower limits), the body-centered cubic (bcc) FM Fe, SrO, and gaseous triplet O<sub>2</sub>. Within the GGA scheme, let  $\mu_{\text{O}}(T, p(\text{O}_2)^{\text{min}}) = 1/2 E(\text{O}_2)^{\text{GGA}} + 1/2 \Delta G(\Delta T, p^{\circ}(\text{O}_2), \text{O}_2) + 1/2 k_{\text{B}}T \ln(p(\text{O}_2)^{\text{min}}/p^{\circ}(\text{O}_2)) = 1/2 E(\text{SrFeO}_3)^{\text{GGA}} - 1/2 E(\text{Fe})^{\text{GGA}} - 1/2 E(\text{SrO})^{\text{GGA}}$ , where  $E(\text{SrFeO}_3)^{\text{GGA}}$ ,  $E(\text{Fe})^{\text{GGA}}$ , and  $E(\text{SrO})^{\text{GGA}}$  are the total energy values of NM SrFeO<sub>3</sub>, bcc FM Fe, and SrO respectively, we acquire  $p(\text{O}_2)^{\text{GGA,min}} = 8.08 \times 10^{-14}$  atm at *T* = 700 K. As to the GGA + *U* situation, the 0.68 eV/O correction is introduced, and the lower limit  $p(\text{O}_2)^{\text{GGA+U,min}}$  is calculated to be 9.86

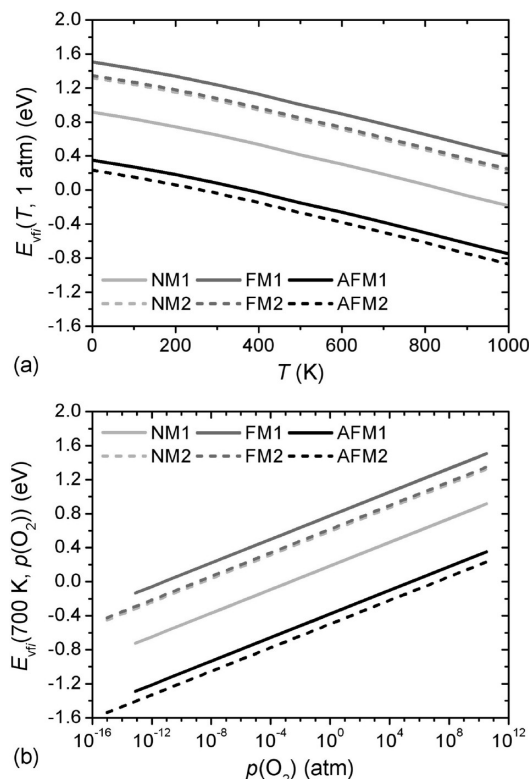


**Figure 10.** O-vacancy formation energy  $E_{vf}(T, p(\text{O}_2))$  ( $i = 1, 2$ ) from  $\text{SrFeO}_3$  to  $\text{SrFeO}_{2.875}$  with different magnetic cases (NM $i$ , FM $i$ , and AFM $i$ ) at (a)  $p(\text{O}_2) = 1 \text{ atm}$  and (b)  $T = 700 \text{ K}$ .

$\times 10^{-16} \text{ atm}$  at  $T = 700 \text{ K}$ , according to  $1/2 k_B T \ln(p(\text{O}_2)^{\text{GGA+U,min}}/p^0(\text{O}_2)) = 1/2 E(\text{SrFeO}_3)^{\text{GGA+U}} - 1/2 E(\text{Fe})^{\text{GGA+U}} - 1/2 E(\text{SrO})^{\text{GGA}} - 1/2 E(\text{O}_2)^{\text{GGA}} - 1/2 \Delta G(\Delta T, p^0(\text{O}_2), \text{O}_2) - 0.68 \text{ eV}$ , where  $E(\text{SrFeO}_3)^{\text{GGA+U}}$  and  $E(\text{Fe})^{\text{GGA+U}}$  are the total energy values of NM  $\text{SrFeO}_3$  and bcc FM Fe  $\text{SrO}$ , respectively, calculated at the GGA +  $U$  level. It is evident that the  $E_{vf}(T, p(\text{O}_2))$  decreases with the increasing  $T$  or decreasing  $p(\text{O}_2)$ . At  $p(\text{O}_2) = 1 \text{ atm}$  for the NM structure, the  $E_{vf}(T, p(\text{O}_2))$  reaches zero around  $T = 850 \text{ K}$ , and  $E_{vf2}(T, p(\text{O}_2)) = 0.22 \text{ eV}$  at  $1000 \text{ K}$ . Regarding the NM cases at  $T = 700 \text{ K}$ , the oxygen-vacancy formation becomes thermodynamically favorable (exothermic) at  $p(\text{O}_2)$  below  $2 \times 10^{-3} \text{ atm}$  within the GGA framework (eq 3) or  $3 \times 10^{-9} \text{ atm}$  at the GGA +  $U$  level with the  $0.68 \text{ eV}/\text{O}$  correction (eq 4). Compared with the data of other systems,<sup>18,29</sup> such ease of oxygen-vacancy formation in  $\text{SrFeO}_3$  accounts for its potentially wide application to catalysis or electrocatalysis (e.g., solid oxide fuel cells), oxygen separation, and sensors.<sup>30</sup>

In view of the difficulty in evaluating magnetic systems using US-PPs,<sup>31</sup> we have chosen additionally another Fe US-PP involving  $3s$  and  $3p$  semicore states with 16 e in total to check some results, and general agreement has been observed. The total energy value of FM  $\text{SrFeO}_3$  obtained with this PP within the GGA scheme is 1.316 and 0.269 eV/fu lower than those in the NM and AFM cases, respectively, and the corresponding values at the GGA +  $U$  level are 2.446 and 0.278 eV/fu. The atomic positions of  $\text{SrFeO}_{2.875}$  relaxed with this PP exhibit only slight divergences from those in Table 1, and the acquired  $E_{vf1}$  values are 0.35, 1.59, and 1.00 eV for the AFM, FM, and NM configurations, respectively,

agreeing very well with the preceding ones. The corresponding  $E_{vf2}$  values of 0.07, 1.29, and 1.09 eV here display seemingly large deviations from the aforementioned results, but considering the around 0.09 eV uncertainty of DFT methods,<sup>32</sup> such differences might be acceptable.

#### 4. Conclusions

Using the PW-PP DFT method, we have calculated the structural, electronic, and magnetic properties of  $\text{SrFeO}_{2.875}$  within the GGA (+  $U$ ) frameworks, taking NM, FM, and AFM patterns into account. By referring to  $\text{SrFeO}_3$ , the vacancy-induced changes have been clarified.

Beyond the NN Fe3, Sr2, and O7 atoms, Sr1, Fe2, O4, and Fe1 in  $\text{SrFeO}_{2.875}$  have undergone observable positional modifications during the relaxation as well though the population analyses reveals that the oxygen-vacancy formation transfers charges predominantly to the Fe3 atoms, especially the  $3d_{z^2}$  and  $3d_{x^2-y^2}$  orbitals for the NM configuration. This also indicates that the constrained relaxation (within the NN region) is insufficient to determine the structures and energetics of this species.

The reduced DOS at  $E_F$  for NM  $\text{SrFeO}_{2.875}$  has been reflected only slightly at the GGA +  $U$  level, while the vacancy-caused localization of the states at  $E_F$  has been verified by the magnetic moments and LDOS results. The states of  $\text{SrFeO}_{2.875}$  at  $E_F$  are found to be  $\pi^*$  for the NM structure and  $\sigma^*$  for the FM and AFM patterns.

With the correction of the  $\text{O}_2$  overbinding error using the value in the literature,<sup>5</sup> the NM and FM cases create similar values of the oxygen-vacancy formation energy at the GGA +  $U$  level, which are much smaller than those of many other oxides, indicative of the easy reduction of  $\text{SrFeO}_3$ . The values in the AFM cases are extremely small, implicating the extraordinary ease of the transform under such a magnetic pattern.

Supplementary calculations using an alternative Fe US-PP involving  $3s$  and  $3p$  semicore states have yielded generally consistent results, indicating that treating only  $3d$  as the semicore states with NLCC seems adequate to represent the present systems.

**Acknowledgment.** This work has been financially supported by the National Natural Science Foundation of China (Grant No. 50730002) and the Knowledge Innovation Program of the Chinese Academy of Sciences (Grant No. KGCX2-YW-362-2).

#### References

- (1) Tsujimoto, Y.; Tassel, C.; Hayashi, N.; Watanabe, T.; Kageyama, H.; Yoshimura, K.; Takano, M.; Ceretti, M.; Ritter, C.; Paulus, W. *Nature* **2007**, *450*, 1062–1065.
- (2) Koslowski, T. *Phys. Chem. Chem. Phys.* **1999**, *1*, 3017–3023.
- (3) Goodenough, J. B. *J. Appl. Phys.* **1966**, *37*, 1415–1422.
- (4) Shein, I. R.; Kozhevnikov, V. L.; Ivanovskii, A. L. *J. Phys. Chem. Solids* **2006**, *67*, 1436–1439.
- (5) Wang, L.; Maxisch, T.; Ceder, G. *Phys. Rev. B* **2006**, *73*, 195107.

- (6) Jaya, S. M.; Jagadish, R.; Rao, R. S.; Asokamani, R. *Phys. Rev. B* **1991**, *43*, 13274–13279.
- (7) Baroni, S.; Dal Corso, A.; de Gironcoli, S.; Giannozzi, P.; Cavazzoni, C.; Ballabio, G.; Scandolo, S.; Chiarotti, G.; Focher, P.; Pasquarello, A.; Laasonen, K.; Trave, A.; Car, R.; Marzari, N.; Kokalj, A. <http://www.quantum-espresso.org> (accessed July 10, 2009).
- (8) Perdew, J. P.; Burke, K.; Ernzerhof, M. *Phys. Rev. Lett.* **1996**, *77*, 3865–3868.
- (9) Monkhorst, H. J.; Pack, J. D. *Phys. Rev. B* **1976**, *13*, 5188–5192.
- (10) Marzari, N.; Vanderbilt, D.; de Vita, A.; Payne, M. C. *Phys. Rev. Lett.* **1999**, *82*, 3296–3299.
- (11) Shanno, D. F.; Phua, K. -H. *Math. Program.* **1978**, *14*, 149–160.
- (12) Blochl, P. E.; Jepsen, O.; Anderson, O. K. *Phys. Rev. B* **1994**, *49*, 16223–16233.
- (13) Löwdin, P. -O. *J. Chem. Phys.* **1950**, *18*, 365–375.
- (14) Bader, R. F. W.; Beddall, P. M. *J. Chem. Phys.* **1972**, *56*, 3320–3329.
- (15) Henkelman, G.; Arnaldsson, A.; Jónsson, H. *Comput. Mater. Sci.* **2006**, *36*, 354–360.
- (16) Choi, Y.; Mebane, D. S.; Lin, M. C.; Liu, M. *Chem. Mater.* **2007**, *19*, 1690–1699.
- (17) Wyckoff, R. W. G. *Crystal Structures*, 2nd ed.; John Wiley & Sons, Inc.: New York, 1963; Vol. 1, pp 10, 16, 90.
- (18) Astala, R.; Bristowe, P. D. *Comput. Mater. Sci.* **2001**, *22*, 81–86.
- (19) Matar, S. F. *Prog. Solid State Chem.* **2003**, *31*, 239–299.
- (20) Kokalj, A. *Comput. Mater. Sci.* **2003**, *28*, 155–168. Code available from <http://www.xcrysden.org/> (accessed July 10, 2009).
- (21) Anderson, P. W. *Phys. Rev.* **1958**, *109*, 1492–1505.
- (22) Shein, I. R.; Shein, K. I.; Kozhevnikov, V. L.; Ivanovskii, A. L. *Phys. Solid State* **2005**, *47*, 2082–2088.
- (23) Pople, J. A.; Gordon, M. H.; Fox, D. J.; Raghavachari, K.; Curtiss, L. A. *J. Chem. Phys.* **1989**, *90*, 5622–5629.
- (24) Hammer, B.; Hansen, L. B.; Nørskov, J. K. *Phys. Rev. B* **1999**, *59*, 7413–7442.
- (25) Reuter, K.; Scheffler, M. *Phys. Rev. B* **2001**, *65*, 035406.
- (26) Di Valentin, C.; Pacchioni, G.; Selloni, A. *Chem. Mater.* **2005**, *17*, 6656–6665.
- (27) Kuwabara, A.; Tanaka, I. *J. Phys. Chem. B* **2004**, *108*, 9168–9172.
- (28) Hodges, J. P.; Short, S.; Jorgensen, J. D.; Xiong, X.; Dabrowski, B.; Mini, S. M.; Kimball, C. W. *J. Solid State Chem.* **2000**, *151*, 190–209.
- (29) Fabris, S.; Vicario, G.; Balducci, G.; de Gironcoli, S.; Baroni, S. *J. Phys. Chem. B* **2005**, *109*, 22860–22867.
- (30) Peña, M. A.; Fierro, J. L. G. *Chem. Rev.* **2001**, *101*, 1981–2017.
- (31) Kresse, G.; Joubert, D. *Phys. Rev. B* **1999**, *59*, 1758–1775.
- (32) Kohn, W.; Becke, A. D.; Parr, R. G. *J. Phys. Chem.* **1996**, *100*, 12974–12980.

CT900405J